Preprint Title	Improving magnetic properties of Mn and Zn doped polyhedral core/shell iron oxide nanoparticles by tuning their size
Authors	Dounia Louaguef, Ghouti Medjahdi, Sebastien Diliberto, Klaus M. Seemann, Thomas Gries, Joelle Bizeau, Damien Mertz, Eric Gaffet and Halima Alem
Publication Date	16 Apr. 2025
Article Type	Full Research Paper
Supporting Information File 1	Louaguef et al._Belstein_J_nanotechnology_supp_info.docx; 333.8 KB
ORCID® iDs	Joelle Bizeau - https://orcid.org/0000-0002-7810-0525; Damien Mertz - https://orcid.org/0000-0002-6745-8978; Eric Gaffet - https://orcid.org/0000-0002-6451-3011; Halima Alem - https://orcid.org/0000-0002-7918-0504

Improving magnetic properties of Mn and Zn doped polyhedral core/shell iron oxide nanoparticles by tuning their size

Dounia Louaguef [1], Ghouti Medjahdi[1], Sébastien Diliberto[1], Klaus M. Seemann[1], Thomas Gries[1], Joelle Bizeau[2], Damien Mertz[2], Eric Gaffet[1] and Halima Alem*[1]

[1] Université de Lorraine. CNRS. IJL, F54011 Nancy. France

[2] Institut de physique et de chimie des matériaux. UMR 7504 CNRS – Université de Strasbourg. France

* corresponding author: halima.alem@univ-lorraine.fr

Abstract:

Superparamagnetic iron oxide nanoparticles (SPIONPs) offer promising applications in nanomedicine due to their appealing properties. Their magnetic and magnetic hyperthermia properties are considered as relevant tools for low invasive cancer therapeutic applications. In this work, we report on the synthesis of polyhedral core/shell SPIONPs. Their size was tuned to improve their magnetic properties. Furthermore, by hybridizing into a core/shell inorganic/inorganic structure, the nanoparticles can achieve significantly improved magnetic-to-thermal energy conversion efficiency (at least of 10 fold). The designed core NPs will then be composed of a core composed of $Zn_{0.4}Fe_{2.6}O_4$ and a shell of $MnFe_2O_4$. Their size and morphology were determined by transmission electron microscopy (TEM), Fourier transform infra- red (FTIR) was used to investigate their chemical composition. The iron oxide phase was confirmed by Mössbauer analysis, and their magnetic properties were studied to select the ideal size for magnetic hyperthermia application.

Keyword: core/shell nanoparticles, magnetic properties, magnetic hyperthermia

I- Introduction:

Magnetic nanoparticles (MNPs) have emerged as a versatile class of materials due to their unique magnetic properties, small size, and biocompatibility, which enable them to be used in a wide range of biomedical applications. These applications include magnetic resonance imaging (MRI), magnetic separation, targeted drug delivery, and hyperthermia for cancer treatment[1,2]. Among these, magnetic hyperthermia has been extensively investigated as a novel cancer treatment due to its ability to locally generate heat in tumors, thereby minimizing damage to healthy tissues compared to conventional chemotherapy and radiotherapy[3]. This process relies on exposing magnetic nanoparticles to an alternating magnetic field (AMF), causing them to generate heat through Brownian and Néel relaxation mechanisms[4]. The heat generation capacity of these nanoparticles is often quantified by the specific absorption rate (SAR), which represents the power dissipated as heat per gram of nanoparticles under the influence of an AMF.

The development of magnetic nanoparticles with enhanced SAR and improved biocompatibility has been a major objective in the field of nanomedicine. Among the various materials used for magnetic hyperthermia, superparamagnetic iron oxide nanoparticles (SPIONs), such as magnetite ($Fe_{3-\delta}O_4$) and maghemite (γ-Fe_2O_3), have been extensively studied due to their low toxicity, biocompatibility, and ease of synthesis[5]. However, SPIONs face several challenges related to their relatively low saturation magnetization (M_s) and specific loss power (SLP), which limit their effectiveness in hyperthermia applications. Consequently, efforts have been made to design new ferrite systems that offer improved performance. One promising strategy involves substituting iron with other divalent cations (M) in spinel ferrites (MFe_2O_4), such as cobalt (Co), manganese (Mn), zinc (Zn), and nickel (Ni), to modify the magnetic properties of the nanoparticles[6] .

A significant amount of research has focused on $CoFe_2O_4$ as a shell material to enhance the magnetic properties of core/shell nanoparticles due to its high coercivity and magnetic anisotropy[7]. The formation of $CoFe_2O_4$ shells on $Fe_{3-\delta}O_4$ cores has been shown to increase the magnetic saturation and improve hyperthermia performance. However, the cytotoxicity of Co-based nanoparticles poses a significant challenge for biomedical applications. Studies have demonstrated that Co^{2+} ions released from these particles can enter the bloodstream and accumulate in organs, where they induce oxidative stress, genotoxic effects, and

inflammation[8,9]. This has raised concerns regarding their use in clinical applications, leading researchers to develop alternative, non-toxic substitutes for Co-based nanoparticles.

In this context, manganese ferrite ($MnFe_2O_4$) has been identified as a promising alternative due to its biocompatibility, high magnetic moment, and potential for use in hyperthermia and drug delivery applications[10] . Manganese is naturally present in the human body and exists primarily as Mn^{2+} and Mn^{3+} ions, making it more biocompatible than cobalt. The substitution of Fe^{3+} with Mn^{2+} in ferrites introduces uncompensated magnetic moments, thereby enhancing the overall magnetic properties[11]. $MnFe_2O_4$ nanoparticles have been reported to exhibit higher SAR and SLP values than $Fe_{3-\delta}O_4$ [4] or $ZnFe_2O_4$ due to the higher magnetic moment of Mn^{2+} ions[10].

While the chemical composition of magnetic nanoparticles is critical, the morphology of the particles also plays a significant role in determining their magnetic properties. Although spherical nanoparticles have been extensively studied, recent research suggests that polyhedral-shaped nanoparticles exhibit superior magnetic performance due to their reduced surface spin disorder [7]. Polyhedral NPs exhibit higher magnetic saturation, reduced spin canting, and higher SAR values than spherical NPs. For instance, Kasparis et al. demonstrated that polyhedral $Zn_{0.4}Fe_{2.6}O_4$ NPs exhibited SAR values more than double those of their spherical counterparts[12]. This observation highlights the importance of morphology control in the design of high-performance magnetic nanoparticles.

One effective approach to achieving both enhanced magnetic properties and biocompatibility is the formation of core/shell structures, where the core provides a strong magnetic moment, and the shell enhances magnetic anisotropy and stability. Core-shell NPs offer a pathway to improving SLP, SAR, and stability under physiological conditions[13]. The core/shell configuration allows for tuning of magnetic properties through the choice of core and shell materials. While $CoFe_2O_4$ shells are known to increase magnetic anisotropy, their cytotoxicity limits their use. In contrast, $MnFe_2O_4$ shells provide a non-toxic alternative that enhances the overall magnetic performance while maintaining biocompatibility.

The orginality of this study lies in the synthesis and characterization of polyhedral $Zn_{0.4}Fe_{2.6}O_4$ nanoparticles and their subsequent transformation into $Zn_{0.4}Fe_{2.6}O_4$@$MnFe_2O_4$ core-shell nanoparticles with tunable sizes. Previous studies have explored core/shell systems with Co-based shells, but our approach employs $MnFe_2O_4$ as the shell material to eliminate the cytotoxicity concerns associated with cobalt. Furthermore, we demonstrate a size-controlled

synthesis strategy by varying the concentration of oleic acid, a surfactant that influences particle size and morphology. This approach enables the synthesis of NPs with sizes ranging from 5 nm to 50 nm, with clear evidence of core/shell formation.

In summary, this study presents a novel approach to the synthesis of core/shell $Zn_{0.4}Fe_{2.6}O_4$@$MnFe_2O_4$ nanoparticles with controlled size and morphology. By incorporating a $MnFe_2O_4$ shell, we achieve significant improvements in magnetic performance while expecting good biocompatibility. The use of size-controlled synthesis enables the exploration of size-dependent magnetic properties, while the direct characterization of the core/shell structure using FT-IR and HR-TEM provides a comprehensive understanding of the material's composition and properties. This work paves the way for the development of next-generation biocompatible magnetic nanoparticles for cancer therapy and other biomedical applications.

II- Materials and methods

a. Materials

Iron acetylacetonate. manganese acetylacetonate and oleic acid were purchased from Aldrich. Zinc acetylacetonate was purchased from Merck KGaA. Benzyl ether 99% from Acros organics. and finally, ethanol absolute anhydrous and toluene were purchased from Carlo ERBA. All the reactants were used as received.

b. Synthesis

i. Synthesis of polyhedral nanoparticles

The core of nanoparticles ($Zn_{0.4}Fe_{2.6}O_4$) was obtained by mixing iron (III) acetylacetonate (0.55 mmol) and Zn(II) acetylacetonate (0.83 mmol) in the presence of oleic acid (the amount of oleic acid was tune depending on the targeted size of the NPs (**see Table 1**) and benzyl ether (52. 61 mmol). The mixture was placed in a 250 ml three-necked round bottom flask and heated at 290ºC for 30 minutes under argon atmosphere. After 30 minutes. the mixture was cooled down to room temperature under ambient conditions. ethanol was added to the mixture forming a black precipitate which was centrifuged (10000 rpm (rotation/min) for 10mn) and washed twice with ethanol and dispersed in toluene.[7]

ii. Synthesis of polyhedral core/shell nanoparticles

The polyhedral $Zn_{0.4}Fe_{2.6}O_4$ nanoparticles were coated with an $MnFe_2O_4$-based shell, targeted to be 5 nm in thickness, by mixing iron(III) acetylacetonate (0.18 mmol) and manganese(II) acetylacetonate (0.33 mmol) in the presence of oleic acid (**see Table 1**) and benzyl ether (52.5 mmol). After adding the $Zn_{0.4}Fe_{2.6}O_4$ nanoparticles suspended in hexane. the mixture was heated to 290ºC and maintained under an argon atmosphere for 30 minutes. The mixture was then cooled to room temperature under ambient conditions. and ethanol was added to produce a black precipitate. The mixture was centrifuged at 10.000 rpm. washed twice with ethanol. and then dispersed in toluene.[7]

Table 1. Volume of oleic acid as a function of NPs targeted average diameter

Core NPs average diameter (nm)	Core/shell NPs average diameter (nm)	Oleic acid Volume (mmol)
5	10	6.3
10	15	5.6
18	22	4.2
45	50	0.7

c. Characterization methods:

Structural characterization of NPs was performed by X-ray diffractometer (XRD) measurements. X-ray diffraction profiles NPs (**Figure 1, Supplementary Information)** were obtained with a PANalytical X'Pert Pro MPD diffractometer. The latter was used in a Bragg–Brentano configuration in reflection equipped with a Cu (Kα radiation. 0.154 nm) anticathode and a high-speed multichannel X'Celerator detector. The sample were placed on a silicon zero-background sample holder. The latter was installed on a rotating spinner for allowing the highest number of grains to be in diffraction position and the XRD patterns were recorded at room temperature. The used oven is Anton Paar 1200N. The powder was placed in a zero-background silicon sample holder and the assembly is placed in the sample holder in the air chamber. The nanoparticles were annealed at 300°C to remove all the traces of the solvent.

Mössbauer analysis **(Figure 2, Supplementary Information))** were performed to determine NPs phase by using a conventional Mössbauer spectrometer in a standard transmission configuration at room temperature. The velocity scale was calibrated with a CoRh (25mCi)

source and a metallic iron foil. The evaluation of the Mössbauer spectra was performed by least-square fitting of lines using the Winnormos (Wissel) program. The error on all of the Fe Mössbauer spectra was ± 0.1 $mm \cdot s^{-1}$.

High resolution Transmission electron microscopy (HR-TEM) and scanning transmission electron microscopy (STEM) images **(figure 1 et 3)** were performed on a JEOL JEM - ARM 200F Cold FEG microscope operating at 200 kV and equipped with a spherical aberration probe corrector (Cs). The chemical compositions were determined by energy dispersive X-ray spectroscopy (EDXS). The X maps were recorded on a Jeol spectrometer (SDD. Jeol DRY SD 30 GV).

NPs Shape and sizes **(Figure 2)** were obtained using a CM200 TEM from Philips with an acceleration voltage of 200kV. a point resolution of approximately 0.27 nm and a magnification from × 50.000 to ×750.000. One drop of a diluted solution of NPs in toluene was deposited on a holey Carbon grid. The latter was heated on a hotplate at 50°C for 2 hours to remove all solvent traces.

The chemical compositions of both core and core/shell NPs were investigated by Fourier transform infrared spectroscopy (FTIR) **(Figure 4).** Both of spectra were recorded using a commercial Agilent FTIR 680 spectrometer in attenuated total reflection (ATR) mode. They were acquired from 400 to 4000 cm^{-1} with a spectral resolution of 4 cm^{-1}. Reference spectra were acquired before each acquisition to determine the absorption spectra in ambient conditions. Each measurement was averaged over 200 scans in continuous mode to improve the signal-to-noise ratio.

Magnetic properties of NPs **(Figure 5)** were studied using a vibrating sample magnetometer (VSM) from Microsense applying a magnetic field of 5KOe. Several mg of purified and surfactant-free NPs were encapsulated into a quartz-glass cup and hermeticallysealed.

The Specific Absorption Rate (SAR) measurement **(Figure 6)** was performed using a calorimetric method on a DM 100 instrument and DM applicator (Nanoscale Biomagnetics™. nB. Zaragoza. Spain) under MaNIaC software (Nanoscale Biomagnetics™).solution of 1 mL of a solution containing the NPs dispersed in toluene (5 mg/mL) was placed in vials adapted for such measurement and an alternating magnetic field of 536.5 kHz / 300 Gauss or 796 kHz / 200 Gauss was applied. The increase of temperature was recorded during 60 seconds. The SAR values was then calculated following the method described by Perigo *et a.l*[14]. the curve

$\Delta T=f(t)$ was fitted with a second-order polynomial function of the form $y=a+b_1*x+b_2*x^2$ where b_1 corresponds to $[dT/dt]_{t=0}$. The SAR value was finally calculated with the following equation:

$$SAR\ (W/g) = \frac{m_{toluene*Cp_{toluene}}}{m_{particles}} * [\frac{dT}{dt}]_{t=0}$$

where $m_{toluene}$ and $Cp_{toluene}$ represent the mass (g) and the heat capacity ($J.g^{-1}.K^{-1}$) of the sample. $m_{particles}$ (g) denotes the mass of the magnetic nanoparticles present in the sample and $[dT/dt]_{t=0}$ is the derivative function of the temperature at t = 0 ($K.s^{-1}$).

III- Results and discussions

X-ray Diffraction Analysis

The XRD pattern (**Figure SI1**) displays sharp and intense peaks characteristic of a well-crystallized material. The most intense peak is located at $2\theta \approx 35.5°$, which corresponds to the (311) reflection, typical of spinel ferrites. Additional peaks were observed at $2\theta \approx 18.3°$, 30.1°, 43.2°, 53.5°, 57.1°, and 62.7°, corresponding to the (111), (220), (400), (422), (511), and (440) planes, respectively. These reflections are in good agreement with the standard spinel cubic phase (space group $Fd\bar{3}m$), matching well with reference data such as JCPDS card No. 22-1012 for $ZnFe_2O_4$. No impurity phases were detected, indicating that the synthesized $Zn_{0.4}Fe_{2.6}O_4$ is a single-phase spinel ferrite. The shift and relative intensity of the peaks may reflect the partial substitution of Fe^{3+} ions by Zn^{2+} ions, which influence the lattice parameters without disrupting the spinel framework.

a- HR- TEM observations

The primary objective of this study was to synthesize core/shell nanoparticles (NPs) with polyhedral morphology and enhanced magnetic properties. The synthesis approach focused on precise control of shape and size, critical factors for tuning magnetic behavior. By employing thermal decomposition, $Zn_{0.4}Fe_{2.6}O_4$ NPs were synthesized with a well-defined polyhedral morphology, as confirmed by high-resolution transmission electron microscopy (HR-TEM) (**Figure 1**). This morphology is critical as polyhedral-shaped NPs have been shown to exhibit

superior magnetic properties compared to spherical particles due to increased surface area and facet effects.

High-resolution TEM images (**Figure 1(a))** reveal well-defined, monodisperse polyhedral $Zn_{0.4}Fe_{2.6}O_4$ nanoparticles with an average size of approximately 40 nm. The size distribution histogram (**Figure 1(b)**) confirms the uniformity of particle sizes, while a magnified image (**Figure 1(c)**) highlights the polyhedral morphology. The selected area electron diffraction (SAED) pattern (**Figure 1(d))** exhibits distinct diffraction spots that can be indexed to the (222), (400), (111), and (311) planes of a spinel-type structure, in agreement with the X-ray diffraction (XRD) data (**Figure SI 1, Supplementary Information**). The presence of the (222) reflection, which is forbidden in XRD for a perfect spinel ($Fd\bar{3}m$) due to structure factor constraints, can be attributed to dynamic scattering effects or local structural ordering, as frequently observed in electron diffraction studies of ferrites. These features collectively indicate a high degree of crystallinity, consistent with previous reports on spinel ferrite nanoparticles.[15]

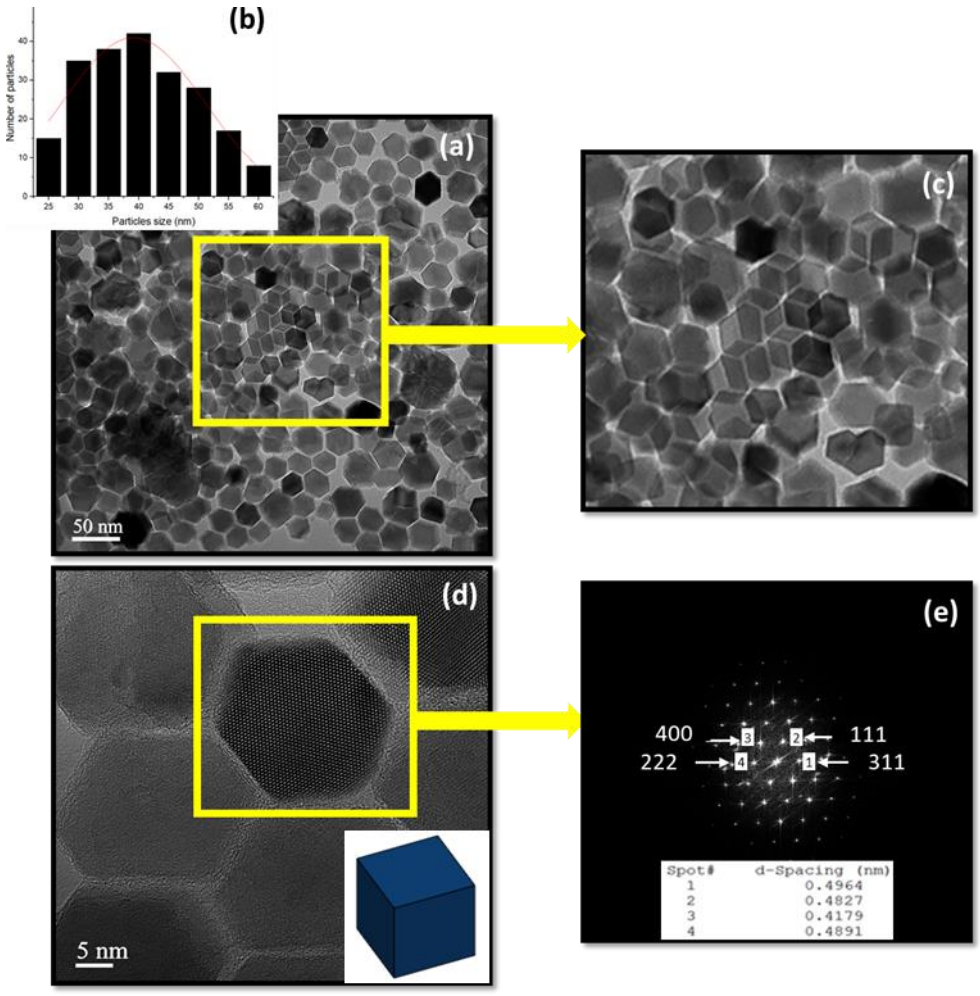

Figure 1 . (a) TEM images (bright field) of $Zn_{0.4}Fe_{2.6}O_4$ NPs (40nm). (b) size distribution histogram of $Zn_{0.4}Fe_{2.6}O_4$ NPs. (c) Zoom on the framed part in yellow (a).(d) HR-TEM image of $Zn_{0.4}Fe_{2.6}O_4$ NPs. (e) Diffraction pattern of the framed part in yellow (d).

To enhance the magnetic properties of $Zn_{0.4}Fe_{2.6}O_4$ nanoparticles (NPs) and $Zn_{0.4}Fe_{2.6}O_4$@$MnFe_2O_4$ NPs based on their size, four distinct sizes were selected as shown in **Table 3**. These sizes were achieved by adjusting the ratio of oleic acid used during the synthesis of $Zn_{0.4}Fe_{2.6}O_4$ and $Zn_{0.4}Fe_{2.6}O_4$@$MnFe_2O_4$ (**see Table 1**). The target average size of these NPs and their polyhedral morphology were confirmed through transmission electron microscopy images (**Figure 2**). The labeled diffraction spots correspond to specific crystallographic planes (e.g., (400), (222), (111), and (311)), confirming the crystalline nature of the nanoparticles. The table (inset in the figure) lists the d-spacing values (in nm), which are consistent with the spinel structure of $ZnFe_2O_4$.

Table 2. Average diameter of $Zn_{0.4}Fe_{2.6}O_4$ and $Zn_{0.4}Fe_{2.6}O_4@MnFe_2O_4$ NPs

$Zn_{0.4}Fe_{2.6}O_4$		$Zn_{0.4}Fe_{2.6}O_4@MnFe_2O_4$	
Diameter (nm)	Image	Diameter (nm)	Image
5±0.4	3.1a	10±1.1	3.2a
10±0.7	3.1b	15±1.03	3.2b
18±1.7	3.1c	22±1.02	3.2c
45±1.2	3.1d	50±1	3.2d

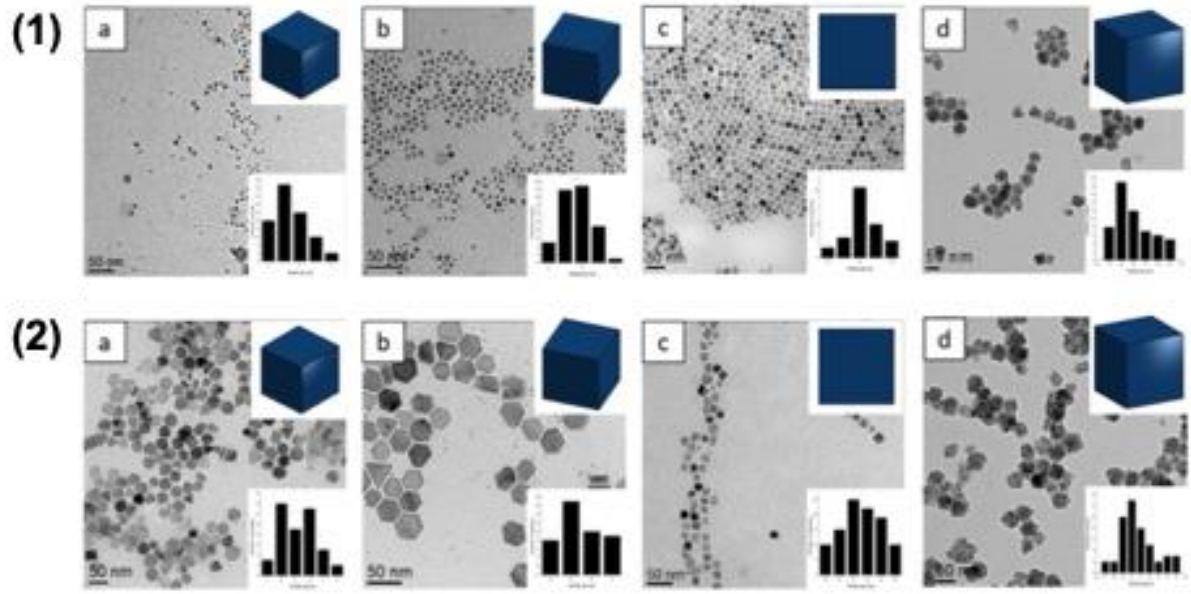

Figure 2. (1) TEM images of $Zn_{0.4}Fe_{2.6}O_4$ NPs (Bright field images) : 5nm (a). 10nm (b). 18nm (c) and 45nm (d). (2) TEM images of $Zn_{0.4}Fe_{2.6}O_4@MnFe_2O_4$ NPs : 10nm (a). 15nm (b). 22nm (c) and 50nm (d).

Elemental analysis using HR-TEM with energy-filtered transmission electron microscopy (EELS) confirmed the elemental distribution within the core and shell of the NPs. As shown in **Figure 3**, Fe, Zn, and O are homogeneously distributed in the $Zn_{0.4}Fe_{2.6}O_4$ NPs (**Figure 3(a)**). For $Zn_{0.4}Fe_{2.6}O_4@MnFe_2O_4$ NPs (**Figure 3(b)**), a clear distinction is observed, where Mn is exclusively located in the shell. This confirms the successful deposition of the $MnFe_2O_4$ shell on the $Zn_{0.4}Fe_{2.6}O_4$ core. Such shell formation has been reported in other studies on core/shell NPs, where the selective deposition of the shell material has been achieved through precise control of synthesis conditions.

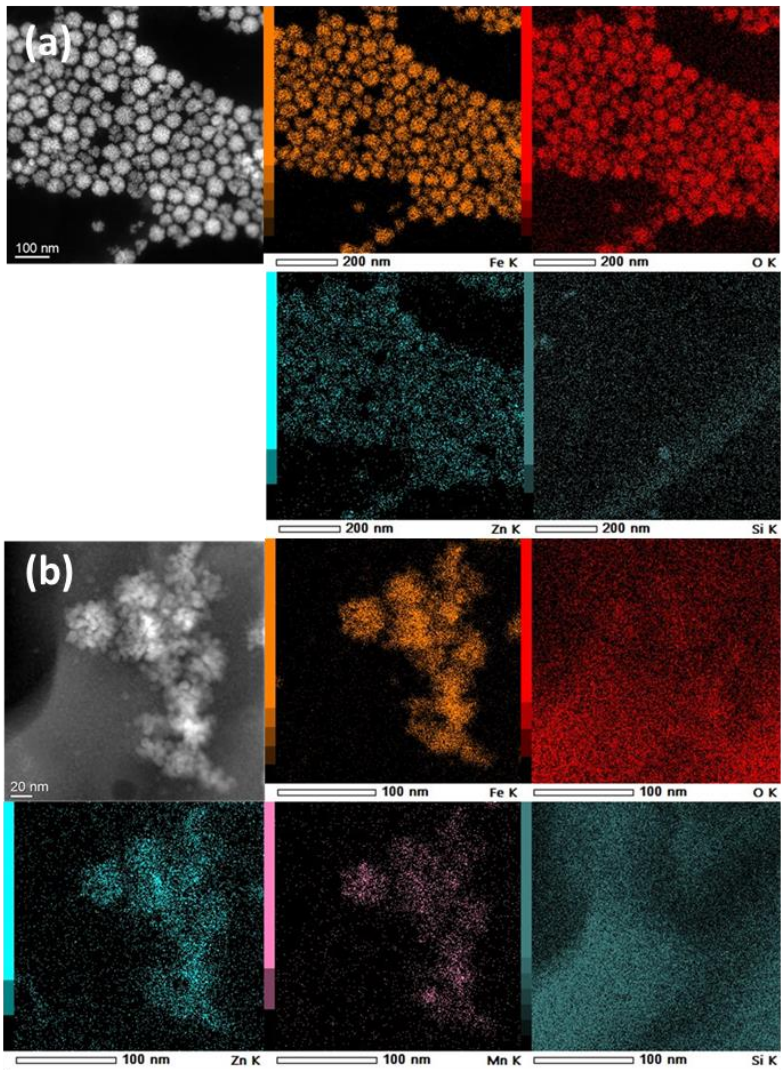

Figure 3. mapping images X of $Zn_{0.4}Fe_{2.6}O_4$ NPs (45nm) (a) and $Zn_{0.4}Fe_{2.6}O_4$@$MnFe_2O_4$ NPs (50nm) (b).

d -IRTF analysis:

The FT-IR analysis of $Zn_{0.4}Fe_{2.6}O_4$ and $Zn_{0.4}Fe_{2.6}O_4$@$MnFe_2O_4$ nanoparticles provides valuable insights into their structural properties and confirms the successful formation of both the core and core/shell structures. The Fe-O stretching vibrations in spinel ferrites typically appear within the range of 500–650 cm^{-1}, with tetrahedral Fe-O bonds generally observed around 550–600 cm^{-1}. However, in the present study, the **$Zn_{0.4}Fe_{2.6}O_4$** sample exhibits a peak at approximately 715 cm^{-1}, significantly higher than expected, and this peak shifts further to 730 cm^{-1} in the $Zn_{0.4}Fe_{2.6}O_4$@$MnFe_2O$ core-shell composite. The higher vibrational frequency in $Zn_{0.4}Fe_{2.6}O_4$ can be attributed to the partial substitution of Zn^{2+} into tetrahedral sites, which strengthens the Fe^{3+}-O bond through enhanced covalency and changes in cation distribution,

leading to shorter and stiffer bonds. The additional upward shift to 730 cm^{-1} in the core-shell structure reflects interfacial strain and electronic interactions between the $Zn_{0.4}Fe_{2.6}O_4$ core and the $MnFe_2O$ shell. This strain distorts the tetrahedral FeO_4 units, further stiffening the Fe-O bonds, while electronic coupling and potential cation redistribution at the interface amplify the vibrational frequency. These structural and electronic effects collectively explain the observed peak positions and their shift, highlighting the impact of lattice distortions, bond strengthening, and interfacial interactions on the vibrational properties of the material[15]. The presence of peaks at **~2850 cm^{-1}** and **~2920 cm^{-1}** is associated with the C-H stretching vibrations from surface capping agents, such as oleic acid, which is commonly used during synthesis to control particle size and prevent aggregation. The broad peak observed at **~3400 cm^{-1}** is linked to the O-H stretching vibrations of adsorbed water or hydroxyl groups on the particle surface, which is a common feature for nanoparticles exposed to ambient conditions.

Although Zn and Mn are present in the $Zn_{0.4}Fe_{2.6}O_4$ and $Zn_{0.4}Fe_{2.6}O_4$@$MnFe_2O_4$ structures, the FT-IR spectrum does not show distinct peaks associated with Zn-O or Mn-O bonds. This absence is due to the nature of the vibrational modes of Zn-O and Mn-O bonds. In spinel ferrites, the strong absorption bands corresponding to the Fe-O bonds at tetrahedral and octahedral sites are significantly more intense than the Zn-O and Mn-O vibrational modes, which have lower dipole moment changes during vibration. As a result, the Fe-O vibrations dominate the FT-IR spectrum. Additionally, Zn^{2+} typically occupies tetrahedral sites in spinel structures, and its associated vibrational modes are often masked by the stronger Fe-O vibrations in this region. Mn^{2+}, which is present in the shell of $Zn_{0.4}Fe_{2.6}O_4$@$MnFe_2O_4$, also occupies octahedral sites and contributes to the overall bonding environment, but its distinct vibrational modes are often indistinguishable due to overlap with the Fe-O modes, especially since Fe^{3+} has a higher mass and stronger dipole moment change compared to Zn^{2+} and Mn^{2+}.

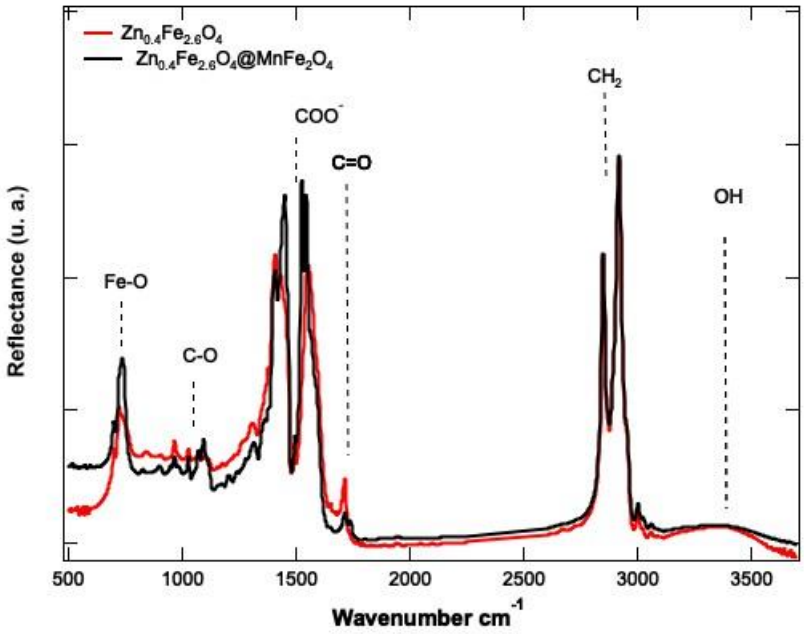

Figure 4. FTIR spectra of $Zn_{0.4}Fe_{2.6}O_4$ NPs (red) and $Zn_{0.4}Fe_{2.6}O_4$@MnFe2O4 (black).

f- Magnetic properties of the core/shell NPs:

The magnetic saturation as a function of magnetic field of $Zn_{0.4}Fe_{2.6}O_4$ and $Zn_{0.4}Fe_{2.6}O_4$@$MnFe_2O_4$ NPs are presented in **Figure 5.** The applied field in this study was 5000 Oe.

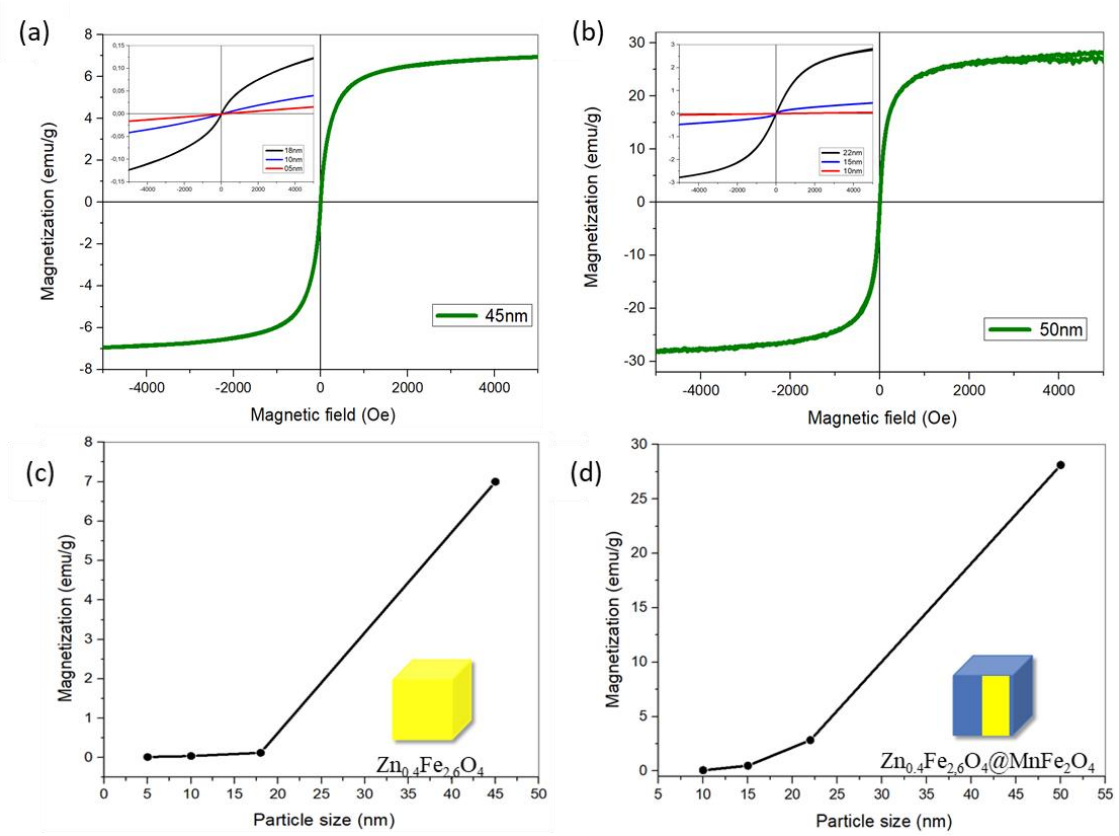

Figure 5. Magnetization curves of $Zn_{0.4}Fe_{2.6}O_4$ NPs (a). $Zn_{0.4}Fe_{2.6}O_4@MnFe_2O_4$ NPs (b). Magnetization as a function of $Zn_{0.4}Fe_{2.6}O_4$ NPs size (c). Magnetization as a function of $Zn_{0.4}Fe_{2.6}O_4@MnFe_2O_4$ NPs size (d).

Table 3 : magnetic saturation values of $Zn_{0.4}Fe_{2.6}O_4$ and $Zn_{0.4}Fe_{2.6}O_4@MnFe_2O_4$ NPs

$Zn_{0.4}Fe_{2.6}O_4$	Magnetic saturation emu / g	$Zn_{0.4}Fe_{2.6}O_4@MnFe_2O_4$	Magnetic saturation emu / g
5.0 ± 0.4 nm (red)	0.012	10.0 ± 1.1nm (red)	0.06
10.0 ± 0.7 nm (blue)	0.031	15.0 ± 1.03 nm (blue)	0.49
18.0 ± 1.7 nm (black)	0.12	22.0 ± 1.02 nm (black)	2.84
45.0 ± 1.2 nm (green)	7.000	50.0 ± 1.0 nm (green)	28.12

The saturation magnetization (Ms) values of $Zn_{0.4}Fe_{2.6}O_4$ nanoparticles (NPs) exhibit a clear size-dependent behavior, with larger particles showing significantly higher Ms. For instance, in

this study, the NPs with sizes of 5.0 ± 0.4 nm, 10.0 ± 0.7 nm, 18.0 ± 1.7 nm, and 45.0 ± 1.2 nm exhibited Ms values of 0.012, 0.031, 0.12, and 7 emu.g^{-1}, respectively. Similar trends have been reported in the literature, where larger particle sizes lead to higher Ms values due to the reduction of surface spin canting and the improved alignment of magnetic moments. For instance, Wang et al. observed that $ZnFe_2O_4$ NPs with sizes ranging from 5 nm to 50 nm displayed Ms values increasing from 1.5 emu/g to 30 emu/g, highlighting the critical role of particle size in magnetic properties[16] .

The role of the core/shell structure in enhancing the magnetic properties of NPs is clearly evident in the case of 45.0 nm $Zn_{0.4}Fe_{2.6}O_4$ NPs and 50.0 nm $Zn_{0.4}Fe_{2.6}O_4$@$MnFe_2O_4$ NPs. In this study, the addition of an $MnFe_2O_4$ shell to the $Zn_{0.4}Fe_{2.6}O_4$ core resulted in a more than fourfold increase in Ms, from 7 emu.g^{-1} for the core alone to 28.12 emu.g^{-1} for the core/shell system.

Furthermore, the superparamagnetic behavior of both $Zn_{0.4}Fe_{2.6}O_4$ and $Zn_{0.4}Fe_{2.6}O_4$@$MnFe_2O_4$ NPs was confirmed by the absence of hysteresis in the magnetization curves. This behavior is characteristic of superparamagnetic NPs, where thermal energy is sufficient to overcome magnetic anisotropy energy barriers, leading to zero remanent magnetization when the applied field is removed. Superparamagnetism is a desirable property for biomedical applications, as it prevents particle aggregation in the absence of an external magnetic field.

g- Magnetic Hyperthermia analysis :

In **Figure 6**, the specific absorption rate (SAR) values of $Zn_{0.4}Fe_{2.6}O_4$@$MnFe_2O_4$ nanoparticles (NPs) are presented as a function of their various sizes: 10, 15, 22, and 50 nm (a). Additionally, the heating curves of 50 nm $Zn_{0.4}Fe_{2.6}O_4$@$MnFe_2O_4$ NPs are shown as a function of time under alternating magnetic fields of 536.5 kHz / 300 Gauss and 796 kHz / 200 Gauss (b).

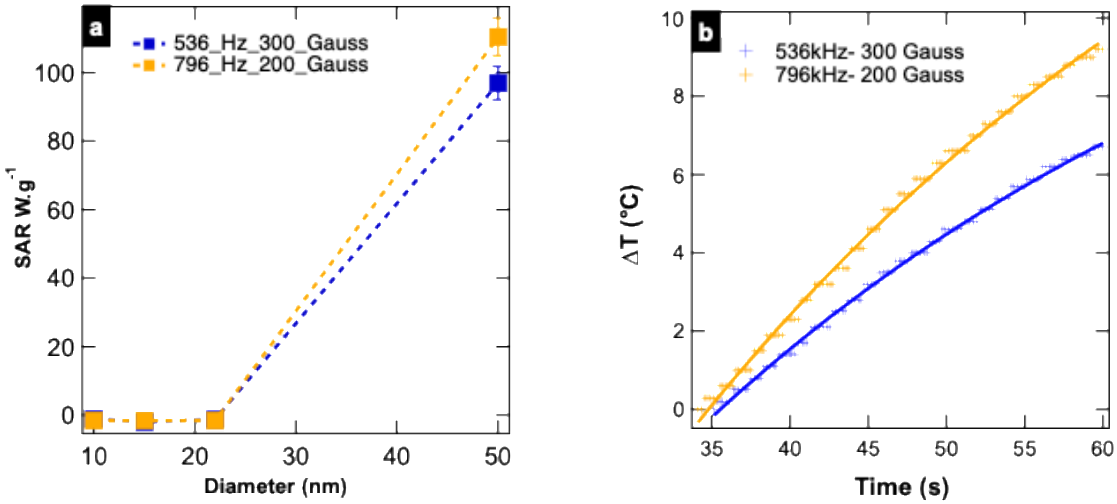

Figure 6. (a) SAR values of $Zn_{0.4}Fe_{2.6}O_4$@$MnFe_2O_4$ NPs according to their different sizes. (b) Heating curves of 50 nm $Zn_{0.4}Fe_{2.6}O_4$@$MnFe_2O_4$ as a function of time under an alternating magnetic field of 536.5 kHz /300Gauss or 796 kHz / 200 Gauss.

The enhanced magnetic hyperthermia performance of the 50 nm $Zn_{0.4}Fe_{2.6}O_4$@$MnFe_2O_4$ core/shell nanoparticles is evidenced by their superior specific absorption rate (SAR) values of 96.92 $W.g^{-1}$ and 110.38 $W.g^{-1}$ under alternating magnetic fields of 536 kHz and 796 kHz, respectively (**Figure 6(a)).** These results are significantly higher than those reported in previous studies involving similar core/shell structures. The observed heating behavior (**Figure 6(b)**) further confirms the effectiveness of these NPs in hyperthermia applications, as demonstrated by a temperature increase of 9.56 °C and 14.42 °C after 60 seconds under magnetic fields of 536 kHz and 796 kHz, respectively.

The superior performance of the $Zn_{0.4}Fe_{2.6}O_4$@$MnFe_2O_4$ core/shell NPs can be attributed to their increased size (50 nm), which is well-documented in the literature to influence hyperthermia performance. For instance, larger NPs often exhibit stronger magnetic responses due to increased magnetic moment and saturation magnetization, which contribute to higher SAR values. Shabalkin et al. reported that $ZnFe_2O_4$@$MnFe_2O_4$ NPs with shell thicknesses of 0.5 nm and 1.7 nm achieved SAR values of only 8 $W.g^{-1}$ under a magnetic field of 100 Oe at 75 kHz, significantly lower than the values obtained in this study[17] . This discrepancy can be explained by the larger particle size of 50 nm used in the present study, as well as the higher frequencies (536 and 796 kHz) applied during the hyperthermia analysis, which are known to enhance energy dissipation through Brownian and Néel relaxation mechanisms.

The role of size in hyperthermia performance has been further highlighted in other studies. It is well established that larger core/shell NPs exhibit enhanced magnetic properties due to increased magnetic anisotropy and moment, both of which contribute to higher energy dissipation. For example, $CoFe_2O_4$@$MnFe_2O_4$ NPs have been shown to achieve SAR values in the range of 210–320 $W.g^{-1}$ under specific magnetic field conditions, demonstrating the effectiveness of core/shell structures in enhancing hyperthermia performance[18]. While the SAR values observed for the $Zn_{0.4}Fe_{2.6}O_4$@$MnFe_2O_4$ NPs in this study are lower than those of $CoFe_2O_4$@$MnFe_2O_4$ NPs, it is important to note that Co-based ferrites typically exhibit higher coercivity and saturation magnetization, which inherently favor higher SAR. However, despite their high SAR values, cobalt-containing nanoparticles are not suitable for biomedical applications due to the well-known cytotoxicity of cobalt ions. Studies have shown that cobalt ions released from nanoparticles can induce oxidative stress, inflammation, and cellular damage, which limits their use in clinical applications. In contrast, Zn and Mn ferrites are known for their lower cytotoxicity and biocompatibility, making them more suitable for biomedical applications. This biocompatibility advantage further emphasizes the potential of $Zn_{0.4}Fe_{2.6}O_4$@$MnFe_2O_4$ NPs for use in hyperthermia cancer therapies.

Another key factor influencing hyperthermia performance is the core/shell structure itself. The core/shell architecture allows for the synergistic combination of the distinct magnetic properties of the core ($Zn_{0.4}Fe_{2.6}O_4$) and the shell ($MnFe_2O_4$), leading to a stronger effective anisotropy and magnetic moment than those observed for single-phase materials. This is consistent with findings from previous reports that show that bimagnetic core/shell NPs exhibit higher SAR values than single-component systems[18]. This enhancement is attributed to the interface exchange coupling effect, which improves magnetic anisotropy and, consequently, the Néel relaxation. In addition, the larger overall size of the NPs favors an increase in Brownian relaxation, which becomes more prominent at higher frequencies.

The heating efficiency of the NPs, as depicted in **Figure 6(b)**, highlights their rapid and sustained heating capability, a critical requirement for hyperthermia applications. The temperature increase of 9.56 °C and 14.42 °C under 536 kHz and 796 kHz, respectively, surpasses the thermal threshold required to induce apoptosis in cancer cells (42–46 °C). The fast heating kinetics observed here are comparable to those reported by Shabalkin et al., where $ZnFe_2O_4$@$MnFe_2O_4$ NPs reached the desired hyperthermic range (42 °C) within seconds under similar field conditions[17] In contrast, other studies with single-phase $MnFe_2O_4$ or $ZnFe_2O_4$ NPs

often require higher magnetic field intensities to achieve comparable heating rates, further confirming the enhanced hyperthermic properties of the core/shell configuration.

Conclusion:

In this study, monodisperse superparamagnetic core/shell iron oxide nanoparticles (NPs) with controlled polyhedral morphology and varying sizes were successfully synthesized via thermal decomposition. The magnetic characterization revealed that larger particles (50 nm) exhibited significantly enhanced magnetic properties compared to smaller counterparts, highlighting the critical influence of particle size on magnetic behavior. Furthermore, the role of the shell was clearly demonstrated, as it contributed to a more than fourfold increase in the magnetic performance of the core/shell NPs relative to the core alone. Hyperthermia analysis further confirmed the excellent heating efficiency of these NPs, with rapid temperature elevation achieved in a short period of time. These findings underscore the potential of core/shell iron oxide NPs for magnetic hyperthermia applications, where precise control of size and shell composition can be leveraged to optimize performance for biomedical use.

.

Acknowledgement

The work was supported by French PIA project “Lorraine Université d’Excellence” reference ANR-15-IDEX-04-LUE and the Algerian Government. This work is based on the Thesis of Dounia Louaguef defended on July 5th 2023 entitled “*Développement de nanoparticules intelligentes type cœur/coquille capables d'encapsuler un médicament pour la thérapie anticancéreuse”* at the University of Lorraine.

References

1. El-Gendy AA. Core/Shell Magnetic Nanoparticles for Biomedical Applications. In: *Magnetic Nanostructured Materials*. Elsevier; 2018:41-58. doi:10.1016/B978-0-12-813904-2.00002-4

2. Salim Albukhaty,Ghassan M.Sulaiman ,Hassan Al-Karagoly et al. Iron oxide nanoparticles: The versatility of themagnetic and functionalized nanomaterials intargeting drugs, and genedeliveries with effectual magnetofection. *J of Drug Delivery Science and Technology* 99 (2024) 105838.doi.org/10.1016/j.jddst.2024.105838

3. Manohar A, Vijayakanth V, Manivasagan P, et al. Investigation on the physico-chemical properties, hyperthermia and cytotoxicity study of magnesium doped manganese ferrite nanoparticles. *Mater Chem Phys*. 2022;287:126295. doi:10.1016/j.matchemphys.2022.126295

4. Chiu-Lam A, Rinaldi C. Nanoscale Thermal Phenomena in the Vicinity of Magnetic Nanoparticles in Alternating Magnetic Fields. *Adv Funct Mater*. 2016;26(22):3933-3941. doi:10.1002/adfm.201505256

5. Vangijzegem T, Stanicki D, Laurent S. Magnetic iron oxide nanoparticles for drug delivery: applications and characteristics. *Expert Opin Drug Deliv*. 2019;16(1):69-78. doi:10.1080/17425247.2019.1554647

6. Pilati V, Cabreira Gomes R, Gomide G, et al. Core/Shell Nanoparticles of Non-Stoichiometric Zn–Mn and Zn–Co Ferrites as Thermosensitive Heat Sources for Magnetic Fluid Hyperthermia. *J Phys Chem C*. 2018;122(5):3028-3038. doi:10.1021/acs.jpcc.7b11014

7. Noh S hyun, Na W, Jang J tak, et al. Nanoscale Magnetism Control via Surface and Exchange Anisotropy for Optimized Ferrimagnetic Hysteresis. *Nano Lett*. 2012;12(7):3716-3721. doi:10.1021/nl301499u

8. Bresson C, Darolles C, Carmona A, et al. Cobalt chloride speciation, mechanisms of cytotoxicity on human pulmonary cells, and synergistic toxicity with zinc. *Metallomics*. 2013;5(2):133. doi:10.1039/c3mt20196a

9. Qiao et Ma - 2013 - Quantification of metal ion induced DNA damage with.pdf.

10. Haque S, Tripathy S, Patra CR. Manganese-based advanced nanoparticles for biomedical applications: future opportunity and challenges. *Nanoscale*. 2021;13(39):16405-16426. doi:10.1039/D1NR04964J

11. Phalake SS, Somvanshi SB, Tofail SAM, Thorat ND, Khot VM. Functionalized manganese iron oxide nanoparticles: a dual potential magneto-chemotherapeutic cargo in a 3D breast cancer model. *Nanoscale*. 2023;15(38):15686-15699. doi:10.1039/D3NR02816J

12. Kasparis G, Sangnier AP, Wang L, et al. Zn doped iron oxide nanoparticles with high magnetization and photothermal efficiency for cancer treatment. *J Mater Chem B*. 2023;11(4):787-801. doi:10.1039/D2TB01338J

13. Salgueiriño-Maceira V, Correa-Duarte MA. Increasing the Complexity of Magnetic Core/Shell Structured Nanocomposites for Biological Applications. *Adv Mater*. 2007;19(23):4131-4144. doi:10.1002/adma.200700418

14. Périgo EA, Hemery G, Sandre O, et al. Fundamentals and advances in magnetic hyperthermia. *Appl Phys Rev*. 2015;2(4):041302. doi:10.1063/1.4935688

15. Rameshbabu R, Ramesh R, Kanagesan S, Karthigeyan A, Ponnusamy S. Synthesis and Study of Structural, Morphological and Magnetic Properties of ZnFe2O4 Nanoparticles. *J Supercond Nov Magn*. 2014;27(6):1499-1502. doi:10.1007/s10948-013-2466-z

16. Wang X, Lv D, Sun L, Wang W, Tu X hang, Ma Z hao. Magnetic behaviors of a ferrimagnetic decorated kagome-like lattice under an external magnetic field. *J Magn Magn Mater*. 2021;538:168259. doi:10.1016/j.jmmm.2021.168259

17. Shabalkin ID, Komlev AS, Tsymbal SA, Burmistrov OI, Zverev VI, Krivoshapkin PV. Multifunctional tunable $ZnFe_2O_4$ @$MnFe_2O_4$ nanoparticles for dual-mode MRI and combined magnetic hyperthermia with radiotherapy treatment. *J Mater Chem B*. 2023;11(5):1068-1078. doi:10.1039/D2TB02186B

18. Valentin Nica , Carlos Caro, Jose Maria Páez-Muñoz *et al*. Bi-Magnetic Core-Shell CoFe2O4@MnFe2O4 Nanoparticles for In Vivo Theranostics. *Nanomaterials* 2020, 10, 907; doi:10.3390/nano10050907